Soft Matter

Cite this: *Soft Matter*, 2011, **7**, 5926

www.rsc.org/softmatter

REVIEW

Microrheology of solutions embedded with thread-like supramolecular structures

David Lopez-Diaz and Rolando Castillo*

Received 17th February 2011, Accepted 28th March 2011
DOI: 10.1039/c1sm05274h

A family of methods uses colloidal particles as a mechanical probe for deforming the medium in conjunction with a procedure to trace the movement of the particles to get rheological information in a very wide frequency range. All of them are under the heading of microrheology. In the last decade, they have been developed up to the point of being a useful tool for understanding the structure and the dynamics of solutions with embedded thread-like supramolecular structures. This is the case of wormlike micellar solutions, which is the main interest of the paper. Here the impact of microrheology has been essential, providing structural information not easily obtained by other methods. Microrheology has also made an important contribution to the understanding of other threadlike system, as in the case of F-actin or fd virus solutions; they will also be discussed.

1. Introduction

Many of the diverse material properties observed in fluid soft materials are related to the complex supramolecular structures embedded in them, which introduce complex dynamics, usually described with multiple characteristic lengths and time scales that can be assessed by different methods. One of the most popular and frequently used methods is rheology, which is employed to examine a broad variety of materials ranging from paints, polymeric formulations, food, biomaterials, surfactant solutions and personal care products, just to mention a few. The rheological response of soft matter materials can be linear or nonlinear depending on the applied stress. Nonlinearity is usually a sign of structural rearrangement in the system by the applied stress or deformation. For systems close to thermodynamic equilibrium, there is always a linear response regime for small enough applied strain or stress. Here, in soft materials, one of the most important properties is the shear modulus, G, which connects the deformation and flow of materials in response to applied stresses, $\sigma = \int_{-\infty}^{t} dt' G(t-t')\dot{\gamma}$. Here, σ is the shear stress and $\dot{\gamma}$ is the shear rate. In contrast with other materials, like

Instituto de Física, Universidad Nacional Autónoma de México, P. O. Box 20-364, Mexico, D. F. 01000. E-mail: rolandoc@fisica.unam.mx

David Lopez-Diaz

Dr David Lopez-Diaz obtained his Doctor in Science (Chemistry) degree at the Universidad de Salamanca, in Spain in 2007. He is finishing a postdoctoral position at the Institute of Physics at the National University of Mexico. His research focuses on the study of molecular structure in complex fluids, and particularly in wormlike micellar solutions.

Rolando Castillo

Professor Rolando Castillo obtained his Doctor in Science (Physics) degree at the National University of Mexico in 1986, where he obtained a permanent position at the Institute of Physics. His research has been focused on simple liquids and complex fluids, and in the past years, he has been focused on rheological properties of wormlike micellar solutions, pattern formation in monolayers, and self-assembled systems. He is the organizer of the Mexican Network in Soft Matter of the Mexican National Council of Science and Technology.

simple liquids or solids, the shear modulus in soft materials exhibit significant time, or frequency, dependence in the range of milliseconds to seconds, or even to minutes. In essence, these materials are viscoelastic, *i.e.*, they exhibit both a viscous and an elastic response. Viscoelasticity properties are usually measured with mechanical rheometers that probe macroscopic samples, *i.e.*, in the milliliter range, in a limited frequency range ($\omega \sim 10^{-2}$–30 rad/s), and in various deformation geometries depending on the extent of strain and the magnitude of shear modulus to be measured. On the other hand, in the last two decades, microrheological techniques[1–11] have been developed up to the point of being reliable to get useful structural and dynamic information in soft materials. Actually, microrheology does not describe a particular technique. The general principle behind microrheology is first, to minimize the mechanical probe that deforms the medium, which is typically a colloidal particle, and second to employ a modern technique to trace the particle probe movement (optical microscopy, light scattering, *etc.*). A colloidal particle is a delicate probe, which introduces a minimum perturbation in the structure and dynamics of fragile soft matter (thermal energies $\sim k_BT$, k_B is the Boltzmann's constant, T is the temperature). This combination allows the measurement of the rheological material properties at the micrometer and submicrometer scales. Therefore, microrheology is a good option when the limitations of standard mechanical rheology are an issue, like the range of frequencies, the size of the shear moduli that can be probed, the sample size, or heterogeneity of specimen to be measured. The aim of this short review is confined to presenting an overview for newcomers on how microrheology can be a useful tool for understanding the structure and the dynamics of solutions with embedded thread-like supramolecular structures. We will be mainly focused on the case of wormlike micellar solutions, although other thread-like systems will also be discussed. Of course, this is a personal point of view of where these kinds of techniques have contributed the most to the understanding of soft matter, and where the most promising developments for the near future are. In the literature, there are excellent reviews focusing on different aspects, as the initial developments and detailed history of the methods,[1–5] more refined techniques and novel applications,[5–9] theory,[10] different descriptions,[7,10,11] and fundamental assumptions behind the generalized Stokes–Einstein relation,[10] *etc.*

2. Methods in microrheology

The basic assumption in microrheology is that the motion of micron-size colloidal particles dispersed within a fluid is determined by the mechanical properties of the surrounding medium, and in a natural way, microrheology has been used to examine the linear response of complex fluids. The experimental methods fall into two classes depending of the forces operating on the probe particles: (1) In passive microrheology, the properties of the material are extracted from the motion of thermally fluctuating colloidal probes. In this group, it is included particle tracking with video microscopy, and diffusive wave spectroscopy (DWS), as well as its extensions like multispeckle DWS. (2) In active microrheology, a probe is actively driven within the material, either in oscillatory or in steady motion by the use of optical tweezers, magnetic tweezers, or atomic force microscopy. As we will mention later, new instruments have been developed where measurements using both kinds of methods are possible. Below, we will describe the most popular methods used in microrheology. Fig. 1 can be of help to understand how the different procedures of data inversion provide the complex shear modulus, starting from different measured quantities. Fig. 2 is a guide of the typical ranges for the shear moduli and frequency that can be obtained with the techniques discussed below that provide good results in fluid soft materials. This figure could be of help to the newcomers to determine which experimental method is the most appropriate for their particular interests. Many experimental details can be found in review papers.[7,11]

2.1. Methods related to direct particle tracking

Fundamental to any kind of experimental method, using probe particles to obtain the rheological response of a complex fluid, is a quantitative modeling of the interaction of the probe with its surroundings. In 1995, Mason and Weitz[12] showed a method where the ensemble average of the position mean-square displacement (MSD), $\langle \Delta \boldsymbol{r}^2(\tau) \rangle \equiv \langle [\boldsymbol{r}(t+\tau) - \boldsymbol{r}(t)]^2 \rangle$, of a colloidal probe particle, due to thermal fluctuations can be related to the properties of the particle's surrounding material; $\boldsymbol{r}$ is the particle position at time t, and τ is the lag time. Here, the motion of a particle of mass m immersed in a complex fluid undergoing Brownian motion is described by a generalized Langevin equation, where the viscoelastic effects are taken into account using a causal time-dependent memory function, $\zeta(t)$.[12,13]

$$m\frac{d\boldsymbol{v}}{dt}(t) = \boldsymbol{f}_R(t) - \int_0^t \zeta(t-\tau)\boldsymbol{v}(\tau)d\tau. \quad (1)$$

Here, $\boldsymbol{v}(t)$ is the particle velocity, and $\boldsymbol{f}_R(t)$ denotes the random Brownian forces acting on the particle. The capability to store energy upon deformation changes the temporal correlations of the stochastic forces acting upon the particle at thermal equilibrium, since the suspending medium must satisfy the fluctuation dissipation theorem $\langle \boldsymbol{f}_R(t) \cdot \boldsymbol{f}_R(t+\tau) \rangle = 3k_BT\zeta(\tau)$. In this method, it is assumed[10–13] that the microscopic memory function

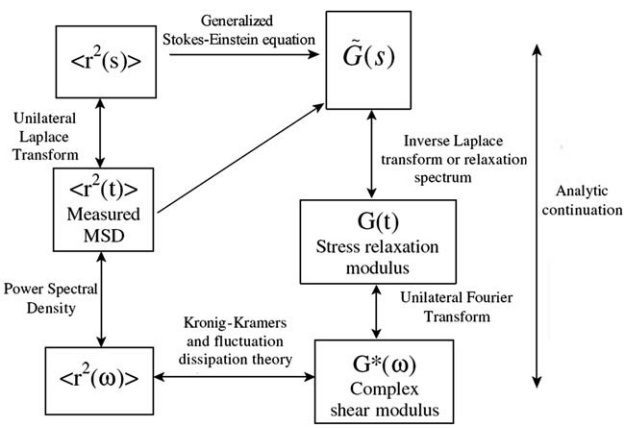

Fig. 1 Different procedures of data inversion used in microrheology to provide the complex shear modulus $G^*(\omega)$ in fluid soft materials, starting from different measured quantities related to the time evolution of the fluctuating position, $\boldsymbol{r}(t)$, of a colloidal probe particle. (Modified figure from Fig. 2 in T. A. Waigh, *Rep. Prog. Phys.*, 2005, **68**, 685.)

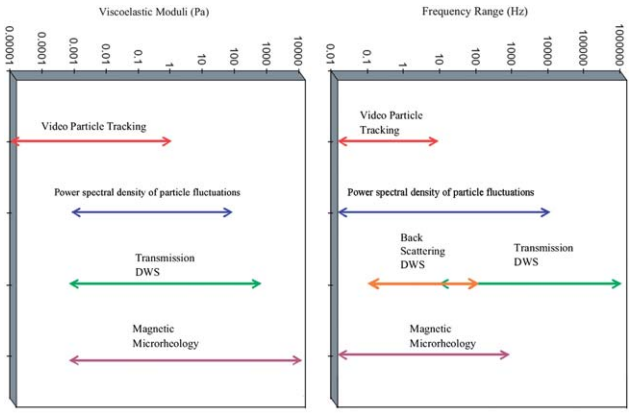

Fig. 2 Typical ranges for the shear viscoelastic moduli (elastic $G'(\omega)$ and viscous $G''(\omega)$ modulus) and frequency that can be measured in fluid soft materials using microrheological methods. (Modified figure from Fig. 1 in T. A. Waigh, *Rep. Prog. Phys.*, 2005, **68**, 685.)

is proportional to the bulk-frequency dependent viscosity of the fluid, $\tilde{\eta}(s) = \tilde{\zeta}(s)/6\pi R$, which is a generalization of the Newtonian fluid behavior. Here, s is the frequency in the Laplace domain. The relation between the Laplace transform of $G(t)$, $\tilde{G}(s)$, and MSD can be written in Laplace space, as:

$$\tilde{G}(s) = s\tilde{\eta}(s) = \frac{s}{6\pi R}\left[\frac{6k_BT}{s^2\langle\Delta\tilde{\boldsymbol{r}}^2(s)\rangle} - ms\right]. \quad (2)$$

Here, R is the probe radius and $\sim$ caps indicate Laplace transform. A generalized Stokes–Einstein equation is obtained neglecting the second term, since inertial effects are negligible when $\omega < 10^6$. A unilateral Fourier transformation, $\boldsymbol{F}_u$, of eqn (2), or employing analytic continuity ($s \rightarrow i\omega$), leads to the complex shear modulus $G^*(\omega)$, which is the Fourier transform of $G(t)$, as a function of frequency:

$$G^*(\omega) = \frac{6k_BT}{\pi Ri\omega\boldsymbol{F}_u\langle\Delta\boldsymbol{r}^2(t)\rangle}. \quad (3)$$

Using this equation in conjunction with particle video tracking gives rise to what is known as single-particle microrheology (1PMR). An extension to this method is the two-particle microrheology (2PMR),[14,15] which is based on multiparticle video tracking to measure the relative vector displacement of tracers. When $r \gg R$, $\tilde{G}(s) = k_BT/2\pi rs\tilde{D}_{rr}(r,s)$. Here, D_{rr} is the diffusion coefficient for correlated fluctuations of two-particle motion along the line connecting them. This method was developed to study heterogeneous materials that have structures typically on length scale of the size of the probe particles. These structures could cause the material to dissipate energy differently from point to point. Therefore, they could be the dominant factor determining a result in a viscoelastic measurement. This new method does not depend on the exact nature of the coupling between the tracers and the medium, and yields accurate rheological data for highly inhomogeneous materials. In addition, it allows examining dynamics at length scales much larger that the probe radius. Therefore, tracking the motion of the probe particles by any experimental technique and using eqn (3), or its extensions (2PMR), leads to passive methods to get $G^*(\omega)$.

2.2. Methods related to the response function or to the power spectral density of position particle fluctuations

In another method, the viscoelastic information of a material can be obtained through an applied force $\boldsymbol{F}$ on an embedded particle, and its resulting displacement $\boldsymbol{r}$; both quantities are related by $\boldsymbol{r}(\omega) = \alpha(\omega)\boldsymbol{F}(\omega)$, in the linear regime. Here, α is the response function, and the various quantities represent the complex Fourier transforms depending on the angular frequency ω. In the absence of any externally applied forces, Brownian motion will give rise to fluctuations of the particle position. These fluctuations are fundamentally related to the temperature of the system and to $\alpha(\omega)$, *via* the fluctuation-dissipation theorem,[16] which relates the imaginary part of $\alpha(\omega)$, denoted by $\alpha(\omega)''$, to the power spectral density of fluctuations of the particle position $\boldsymbol{r}$, by:

$$\left\langle\left|\boldsymbol{r}(\omega)\right|^2\right\rangle = \frac{2k_BT\alpha''(\omega)}{\omega}. \quad (4)$$

Provided that these quantities can be measured over a wide enough frequency range, the Kramer–Kronig integral relation[16] allows the determination of the real part of $\alpha(\omega)$, denoted by $\alpha(\omega)'$, and then the full complex response function $\alpha(\omega)$. A small error could be expected from the finite integration limits in the integral; however, this error is in general negligible when a high frequency sampling rate is used.[17] $G^*(\omega)$ can be related to $\alpha(\omega)$ using[18–20] $\alpha(\omega) = 1/6\pi RG^*(\omega)$, where $G^*(\omega) = G'(\omega) + iG''(\omega)$ is complex and frequency dependent. In oscillatory experiments, the real part of $G^*(\omega)$, the storage or elastic modulus $G'(\omega)$, is in phase with the applied shear strain and the imaginary part of $G^*(\omega)$, the viscous or loss modulus, $G''(\omega)$, is in phase with $\dot{\gamma}$. A typical example of this kind of measurements can be seen in Fig. 3 for a WM solution (details about the WM solutions are given below).

In the same line of thinking, another possibility is to apply controlled external forces to the probe particle to get the response function $\alpha(\omega)$. This can be done through the simultaneous measurement of both, an applied calibrated periodic force $\boldsymbol{F}(\omega)$ and the resulting displacement $\boldsymbol{r}(\omega)$, including any phase shift between them, to finally evaluate $\alpha(\omega)$; this leads to active methods. Optical tweezers can be used to exert forces or drag a trapped particle to mechanically deform the embedding medium. In an optical trap, mechanical forces ($\sim$ 0.1–100 pN) can be readily applied with nanometer position resolution. Such forces have to be quantified prior modeling the optical trap as a linear spring, by measuring small particle displacements from the center of the trap, and by calibrating the trap stiffness. This stiffness depends in part on the refractive index and size of the particle, the wavelength of the trapping light, the dimensions, and photon flux in the trap focus, as well as on the optical properties of the surrounding medium. When an optical trap is employed, the particle is physically held inside a detection zone, avoiding traditional particle tracking complications associated with a freely diffusing particle exiting the field of view. Optical tweezers can also passively monitor the motion of a trapped particle resulting from thermal forces.[21]

New instruments using optical tweezers have been reported where both passive and active microrheology can be performed in the same probe particle,[22–24] through the proper disposition of two collinear lasers for generating two optical traps. One of them is used to drive the particle, which creates a sinusoidally oscillated

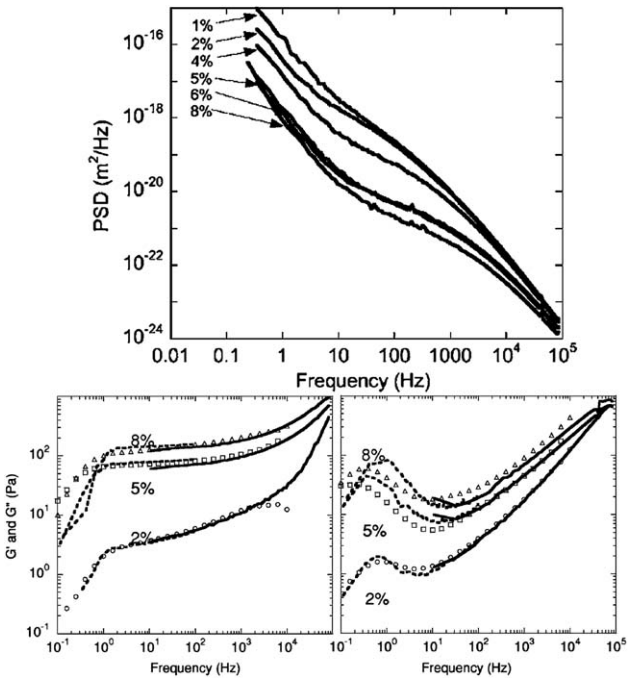

Fig. 3 Typical microrheology results using power spectral densities of position particle fluctuations in a WM solution made of equimolar quantities of CPyCl and NaSal in salty water, at different surfactant concentration in wt%. Upper panel: Power spectral densities as a function of the frequency. Lower panel: Elastic modulus $G'(\omega)$ (left) and viscous $G''(\omega)$ modulus (right) obtained by use of the Kramers–Kronig integral. Solid and dashed lines correspond to different sampling rates, 195 and 20 kHz, respectively. Symbols are macrorheology results obtained with a piezorheometer. (Modified figure from Fig. 3 and Fig. 4 in M. Buchanan, M. Atakhorrami, J. F. Palierne, F. C. MacKintoch, C. F. Schmidt, *Phys. Rev. E.*, 2005, **72**, 11504.)

optical trap. The other laser generates a stationary trap, which is used to sensitively detect the position the particle by using back-focal-plane interferometry. In this way, it is possible to reach resolution of nanometer-level distortions and high-frequency responses, up to ~10 kHz, not accessible with video particle tracking, which is typically limited to ~10 Hz. In comparison, using traditional video particle tracking methods, the particle location measurement is limited in spatial and temporal resolution. Traditionally, magnetic tweezers have been used in active microrheology because they can explore higher force levels than optical tweezers. An example of magnetic tweezers is in ref. 25, and for a comparison among different tweezers see ref. 26. However, optical tweezers are increasingly finding new active microrheology applications, because of their versatility and ability to precisely position beads in locations of interest. Simultaneous manipulation with optical tweezers of multiple beads, whose surface chemistry can be easily modified, could allow the measurement of different interactions between the beads and the surrounding medium; this is a promising line of research in the future.

2.3. Methods of particle tracking related to light scattering

In DWS, the Brownian motion of probe particles incorporated in the fluid of interest is tracked with multiple dynamic light scattering; the particles in the fluid are in a concentration that makes it turbid. Here, photons are multiply scattered and lose their q-dependence. This leads to instruments using only transmission or back scattering geometries. DWS connects the temporal electric field fluctuations of the scattered light emerging from the turbid suspension, characterized by the time averaged field autocorrelation function (ACF), $g^{(1)}(\tau) = \langle E(0)E^*(t)\rangle/\langle|E(0)|^2\rangle$, to the motion of the particles incorporated in the fluid. That is, the MSD of the probe particles can be determined by collecting the scattered intensity from a single speckle of scattered light, over a sufficiently long collection period, to allow the evaluation of the time-averaged light intensity ACF, $g^{(2)}(\tau)$. This measured ACF is related to $g^{(1)}(\tau)$ through the Siegert relation: $|g^{(2)}(\tau)| = 1 + \beta|g^{(1)}(\tau)|^2$, where β is an instrumental factor determined by the collection optics. When all the scattering particles suspended in the fluid are free to explore the same local environment during the course of a measurement, the scattering process is ergodic, and time-averaged ($<\ldots>_T$) and ensemble-averaged ($<\ldots>_E$) correlation functions are identical. In a transmission geometry, the fluid under investigation with the scattering particles immersed in it, can be treated as a slab with an infinite transverse extent and a thickness $L \gg l^*$, where l^* is the transport mean free path. After travelling a l^* distance light is randomized, and the transport of light in a turbid medium can be described by the diffusion approximation.[27–29] In this case, the expression of the time averaged field ACF, $g^{(1)}(\tau)$, is a function of the MSD, the wave vector of the incident light, k_0, and l^*, *i.e.*, $g^{(1)}(\tau) = g^{(1)}(\langle\Delta r^2(\tau)\rangle, k_0, l^*)$.[27–29] Therefore, the MSD of the particles can be extracted from the experimental $g^{(1)}(\tau)$, because l^* is normally determined in an independent measurement, or it can be determined using DWS in transmission geometry for suspensions where the properties of the particles are known.[30–32] Finally, by using eqn (3) the modulus $G^*(\omega)$ can be obtained. A typical example of this kind of measurements can be seen in Fig. 4 for a WM solution (details about the WM solutions are given below).

The available frequency range for $G^*(\omega)$ using DWS is $\sim 10^{-2}$–10^6 rad/s, allowing rheological measurements in complex fluids at high frequencies that are impossible with traditional mechanical measurements.[9] An important extension of DWS has been made, which is called multispeckle DWS. This method was developed for studying systems with slowly evolving transient behavior, exhibiting both short and long relaxation times, up to the point that ergodicity of the media is not assured, *i.e.*, $<\ldots>_T \neq <\ldots>_E$. When this occurs an essential problem ensues, because ensemble averaged quantities are commonly calculated theoretically, while in experiments measurements are usually done by time averaging. The method to correctly measure the ensemble-averaged intensity ACF is based on two ingredients: (a) the multiplication rule,[33] which is based on the idea that light transmitted through a sandwich of two turbid cells can be considered ergodic even though only the second cell is ergodic. If absorption and/or leakage of light take place at the interface between the cells, the multiplication rule relates the intensity ACF of light transmitted through the double-cell sandwich to the ACF of individual cells by a simple multiplication. (b) The use of a CCD camera in transmission geometry,[34] as a multispeckle light detector to allow the simultaneous calculation of several hundreds of correlation functions, where each correlation function is started at a different

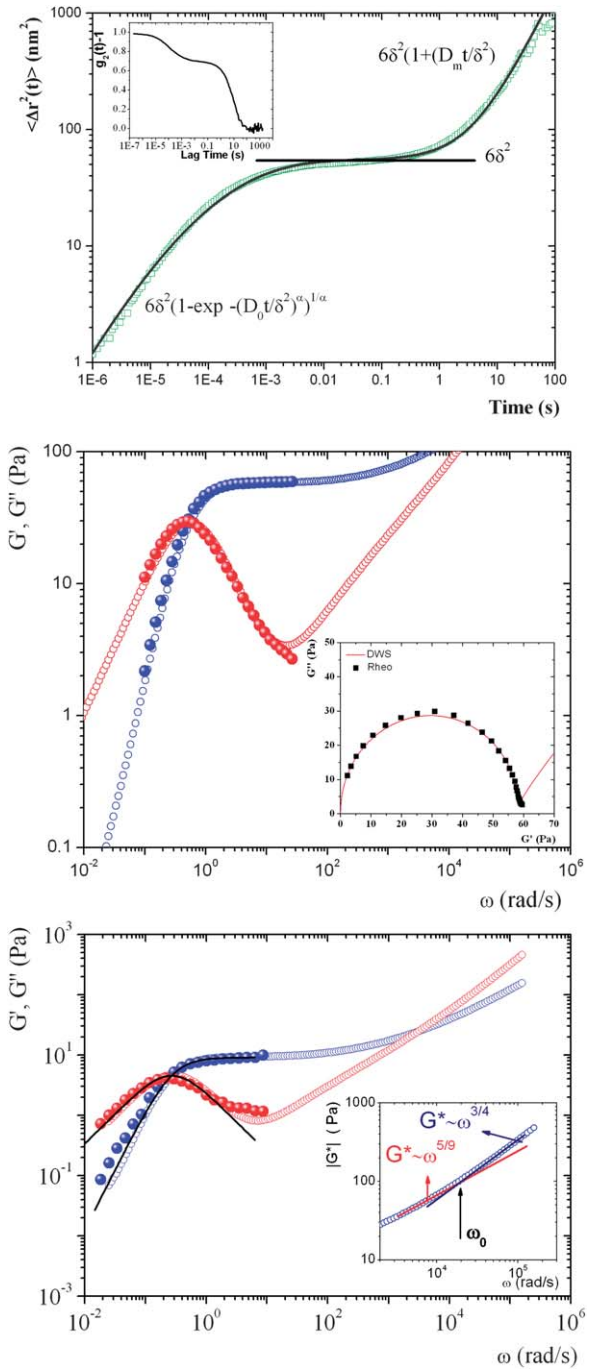

Fig. 4 Microrheology results in a WM solution using DWS. Upper panel: Typical MSD curve as a function of time coming form the light intensity ACF $g^{(2)}(\tau)$ presented in the inset for WMs made of CTAB and NaSal in salty water. The solid line over the experimental points (squares) is the best fit to eqn (5); the main terms of this equation are presented in the figure. Medium panel: Elastic modulus $G'(\omega)$ (blue open circles forming a plateau) and viscous modulus (red open circles), obtained from the MSD presented in the upper panel by using Eq, 3 on the best fit to eqn (5). Solid spheres correspond to results of mechanical rheology presenting the typical behavior of a Maxwell fluid. Inset: A typical Cole-Cole diagram $G''(\omega)$ *vs.* $G'(\omega)$ producing a semicircle when the fluid behaves as a Maxwell fluid, at low and intermediate frequencies. Lower Panel: Typical moduli for WMs made of TDPS and SDS in salty water and the best fit to the $G''(\omega)$ and $G'(\omega)$ expressions of a Maxwell fluid (lines). Inset: The change of slope from 5/9 to $^3/_4$ of $|G^*(\omega)|$ at ω_0. (Modified figure from Fig. 4 in J. Galvan-Miyoshi, J. Delgado, R. Castillo, *Eur. Phys. J. E*, 2008, **26**, 369, and from Fig. 5 in E. Sarmiento-Gomez, D. Lopez-Diaz, R. Castillo. *J. Phys. Chem. B.*, 2010, **114**, 12193.)

time. The multispeckle nature of the CCD camera detector means that a true ensemble average is calculated; no time averaging is necessary.

2.4. Compatibility of measurements and future developments

When one type of response function is measured in the linear response regime, there is a well defined formalism to transform one rheological measured quantity into another.[10] Standard transformations allow $G^*(\omega)$ common in mechanical rheology, where oscillatory stress as a function of strain or viceversa are usually measured, to be transformed into $G(t)$, which comes from the stress relaxation following a fast deformation experiment, or into the compliance, coming from creep under a constant stress experiment. Therefore, the information obtained by microrheology can be translated into the different ways of treating the rheological information.

It is important to mention that microrheology is in constant development. There are important contributions that in the future could be of great significance. Some examples can be mentioned. The extension of DWS to describe the crossover between the single scattering and the diffusive regimes[35] probably will impact biological imaging applications. The microrheological characterization of anisotropic materials using particle tracking[36] could influence many areas of soft materials, like those related to liquid crystals, biopolymer gels, *etc.* There is a theoretical proposal for estimating the frequency-dependent shear viscosity in complex fluids, from the behavior of the velocity autocorrelation function of suspended Brownian particles in a limited time interval, which is determined by the viscous relaxation time of the particles.[37] An active method has been proposed to measure the stress coefficients of complex fluids that represents a first quantitative measurement of a nonlinear rheological property with microrheology.[38] Quite recently, an experimental procedure has been reported using microrheological measurements with optical tweezers, where a generalized Langevin equation is adopted for relating the time-dependent trajectory of a particle in an imposed flow, to the frequency-dependent moduli of a complex fluid. This procedure allows measuring the frequency dependent material linear viscoelastic properties.[39] Probably in the future holographic optical trapping[40] would be more popular in microrheology, because it is a method for applying precisely controlled forces to microscopic objects, where a computer-generated hologram is imprinted onto the wavefronts of a laser beam using a diffractive optical element. The modified beam then is relayed to a high-numerical-aperture lens, which focuses the light into the desired pattern of optical traps. This three-dimensionally structured light field induces the motion of illuminated objects through a combination of induced-dipole forces that arise from local intensity gradients, and radiation pressure, which is directed by local phase gradients. Particle tracking microrheology has been also extended to the study of fluid interfaces; a review of this issue

can be found in ref. 41. Another promising contact with optical microrheology can occur in the future with related techniques, as those involving the recent attempts to develop active electrical microrheology,[42–44] where electric-field-induced displacement of charged spherical colloids embedded in hydrogels can simultaneously measure the viscoelastic properties of the matrix, and the physicochemical characteristics of the probe particles.

Microrheology is based upon the assumptions that the complex fluid can be treated as a continuum around the particle (with non-slip boundary conditions), *i.e.*, the length scales of the network where the particle is embedded are smaller than the size of the particle, and that the Stokes relation for viscous fluids can be extended to describe the viscoelastic drag on a sphere at all frequencies. However, if some of these assumption fails, one cannot generally expect agreement between microrheology and macrorheology measurements. This occurs when the system is out of equilibrium, non-homogeneous, anisotropic, or when strong probe-material interactions are present, just to mention a few. A detailed discussion of when the generalized Stokes–Einstein relation breaks down can be found in ref. 10. 2PMR has helped to deal with some of these problems. However, in some cases a failure in some of the assumptions could encode new rheological information that is inaccessible to macroscopic rheometry, which could motivate to develop new techniques. To this end, theory must be developed to take into account the effects related with the finite size of the probe particles, and its connection with the characteristic lengths of the thread-like structures where the particles are embedded, as well as the effects associated with the boundary conditions over the particle surface. A step in that direction has been presented recently[45,46] by using non-Markovian diffusion equations, which helps to understand the finite-size effects and confinement, as well as hydrodynamic interactions.

3. Wormlike micelles

3.1. Structure and length scales

The study of structure, equilibrium behavior, and rheology of fluids with embedded long linear and flexible tubular aggregates formed by self-assembly of surfactants molecules, better known as wormlike micelles (WMs) has a long history. This can be examined in several review articles.[47–52] WM fluids have been investigated because of their intriguing properties, such as their response to mechanical perturbations, which is viscoelastic, their analogies with polyelectrolytes and polymers, their non-linear rheological behavior with a plateau in the shear stress (σ) *vs.* shear rate ($\dot{\gamma}$) flow curve where in many cases shear banding is observed,[53–56] and because solutions with embedded WMs have become important since their applications cover a wide spectrum:[48] fracture fluids, drag reducing agents, templates for material systems, products of personal care, and household products.

In solution, amphiphilic molecules self-assemble to form various supramolecular structures,[50] the geometry of which can be spherical, cylindrical, lamellar, *etc.* The preferred geometry is fixed by the spontaneous curvature determined by the most effective packing of the assembled aggregates. Therefore, the organization within these supramolecular structures will depend on a complex interplay of molecular geometry, amphiphilic character, and charge of all the involved molecules in the supramolecular structures. This interplay can be modified by many factors as surfactant concentration, added cosurfactants or hydrotope salts, as well as pH, temperature, and ionic strength of the media. The preferred interfacial curvature optimizes the system energetically but does not account for the effects of entropy. At low concentration, below the critical micelle concentration (CMC), entropy favors uniform dissolution of the amphiphile in the solvent, so that both self-assembly and aggregation are negligible. Above the CMC, interaction dominates and entropy effects are reduced. Consequently, the number of aggregates, usually spherical, sharply increases. Cylindrical micelles with a diameter d, are formed by amphiphiles with moderate spontaneous curvature (higher than those that form bilayers, but lower than those that form spherical micelles). In these aggregates, energy is optimized when the curvature is uniform everywhere, forming long linear structures (WMs). However, the system entropy introduces a degree of randomness through bending of the cylindrical micelles, which adds conformational entropy in a manner similar to the configurational entropy of polymeric chains, and through topological defects, in the form of end-caps and/or branch junction points. These two defects are introduced by the formation of regions with differing local curvatures, but incurring different energetic penalties. The overall entropic gain associated with end-caps is greater than that of branch points. Although the appearance of topological defects introduces an entropy gain, the type of defect that dominates the system is set by the amphiphile spontaneous curvature. If the scission energy, E_{sc}, of a micelle (the energy required to create two end-caps from an infinite cylinder) is large enough, then the semi-flexible linear micelles may become very long and entangled, at relatively low total surfactant volume fraction. The distance between entanglement points along a WM will be denoted by l_e (see Fig. 5). End-caps increase entropy by increasing the number of micelles in a given system. Thus, lowering the scission energy shortens the linear micelle contour length, L_c (see Fig. 5). On the other hand, branch junction points increase the number of possible configurations, enabling percolation, and the formation of extended micellar networks, which leads to a multi-connected rather than an entangled cylindrical micelle network.

A key difference of WMs with respect to polymers, where molecular weight distribution is quenched at time of the synthesis, is their equilibrium nature as they constantly break and reform. In WMs, molecular weight distribution is in thermal equilibrium. Small changes in surfactant structure, counterion type and concentration, added electrolytes, or temperature can alter their L_c, the flexibility measured through the bending modulus defined by $\kappa = l_p k_B T$ (l_p is the persistence length, see Fig. 5), and the interaction among them, resulting in pronounced changes in the rheological properties. Theory of WM systems is far from being complete, and it is dominated by the reptation-reaction model and its extensions,[57–60] which are a generalization of the reptation model that successful describes the dynamics of non-breakable polymers. In the fast breaking limit, stress relaxation decays exponentially with a single relaxation time at low and intermediate frequencies, $G(t) = G_0 \exp(-t/\tau_M)$, as in a Maxwell fluid. Here, the reptation-reaction model proposes that the relaxation time, τ_M, is the geometric mean of two characteristic times: for micellar breaking and recombination, τ_b, and for micellar reptation, τ_R, where τ_b must be much smaller

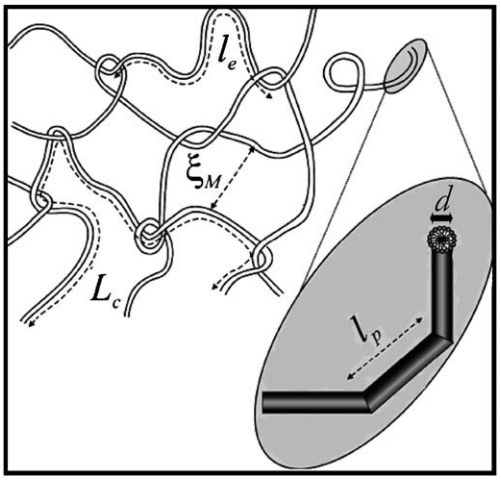

Fig. 5 The most important characteristic lengths in a thread-like network. Linear contour length, L_c, persistence length l_p, entanglement length l_e, mesh size ξ, and diameter d of the filamentous structures. (Modified figure from Fig. 1 in B. A. Schubert, E. W. Kaler, N. J. Wagner, *Langmuir*, 2003, **19**, 4079.)

than τ_R. τ_R represents the time needed for a chain to completely disengage from its original tube by diffusing a distance of the order of L_c. τ_b is the lifetime of a micellar end before it undergoes a recombination reaction. In consequence, all tube segments relax at the same time rate and there are no dispersion of relaxation times.[57–60] In fact, a single relaxation time at low frequencies is a so distinctive WM characteristic that if an unknown micellar systems has this property, the first assumption about its structure is to consider the presence of WMs. Typically, $G_0 \sim$1–1000 Pa denotes the elastic modulus and $\tau_M \sim$ 1 ms–1000 s; $\eta_m = \tau_M G_0$. Therefore, in a good approximation at low and intermediate frequencies (ω < 100 rad/s), WM solutions are viscoelastic, and similar to a Maxwell fluid (See Fig.4b and 4c), *i.e.*, in the corresponding time range (t >10 ms) a single relaxation time dominates,[47–49] and the stress relaxation decays exponentially with a single relaxation time. Translating the stress relaxation to the frequency domain gives: $G^*(\omega)=G_o i\omega\tau_M/1 + i\omega\tau_M$ (See Fig. 4c). A Cole-Cole plot of $G''(\omega)$ *vs.* $G'(\omega)$ produces a typical semicircle in Maxwell fluids (See inset of Fig. 4b).

At high frequencies, where time scales are shorter than those of WM breakage time, the Maxwellian stress relaxation processes are essentially frozen, and the micelles can be regarded as semiflexible polymer chains. Stress relaxes *via* intramicellar processes: First, it is dominated by the Rouse-Zimm modes and then by the internal relaxation of individual Kuhn segments. At this frequency range, G^* exhibits a power-law behavior, $G^* \sim \omega^{\nu}$, with the exponent $\nu \sim 5/9$ in the Rouse–Zimm regime, which changes to $\nu \sim {}^3/_4$, where the internal bending modes of Kuhn segments dominate. This change occurs at a critical frequency,[61] ω_0, corresponding to the shortest relaxation time in the Rouse–Zimm spectrum (See Fig.4c).

3.2. Impact of microrheology in determining the WM length scales

One of the most important contributions of microrheology to the study of WM systems is that G^* (ω) can be experimentally acquired, at high frequencies and with enough precision (See Fig. 3 and 4), allowing to estimate the most important characteristic lengths of the WM network, using approximate relations coming from theory. The characteristic lengths of major interest to understand the structure and dynamics of WM micelles are L_c, l_p, l_e, and the mesh size ξ (See Fig. 5). Once microrheology provides $G^*(\omega)$, the WM network mesh size can be calculated from[58] $\xi = (k_B T/G_0)^{1/3}$; the WM persistence length can be obtained directly from[61] $\omega_0 \approx k_B T/8\eta_m l_p^3$. The contour length can be obtained from the equation $G''_{min}/G_0 \approx l_e/L_c$.[60] Where $G''_{min}$is the local minimum of $G''(\omega)$ after the first crossing between $G'(\omega)$ and $G''(\omega)$; G''_{min}/G_0 must be less than 0.1 to produce relatively good values of l_e/L_c. l_e can be computed using[60] $l_e = \xi^{5/3}/l_p^{2/3}$. The only distance that cannot be obtained with microrheology is the diameter of the WM. Although, this d can be estimated, from the length of the surfactant tails involved in the WM.

High frequency microrheology constitutes a major step forward because it is an excellent alternative to standard techniques, as small-angle neutron scattering (SANS) to obtain structural information in WM solutions. In neutron scattering, thanks to the excellent contrast of hydrogenated surfactants in deuterated water, neutron scattering spectra (measured neutron scattering intensity *vs.* wave vector, q) of WM solutions can be obtained and compared with the scattering spectra of theoretical models of assemblies of disordered cylindrical micelles. The scattering curves involve information about overall size and mass (apparent radius of gyration and apparent molar mass) at the lowest q, flexibility (l_p) in the intermediate q range, and local structure at higher q (d, and the mass per length of the cylindrical micelle).[51] With this technique d, l_p and in some cases, l_e and L_c can be obtained,[49,62–67] although most of the times in conjunction with other techniques, as mechanical rheology and rheooptics.[64] However, neutron scattering needs the use of complex facilities to make the experiments, and an elaborate data treatment. In contrast, in microrheology standard laboratory equipment is needed. The net result is that SANS have provided WM characteristic lengths in limited number of cases, and in very particular thermodynamic states, and it is not very practical to make systematic studies, as those needed to understand the whole picture in WM systems. Examples of characteristic length obtained with SANS can be found in refs. 49, 62–67 and in Table 1 of ref. 51. Other techniques where l_p can be obtained are neutron spin echo,[68,69] birefringence measurements[70] where the knowledge of the stress-optical coefficients are not always accessible, or in some cases through the use of dynamic light scattering.[71]

3.3. Studies of microrheology in wormlike micelle solutions

In the development of WM solutions microrheology, we can observe two stages. In the first one, the methods were in a permanent validation. In a second one, the methods are starting to be used as a tool to get structural and dynamical information about the WMs. In 2000, van Zanten and Rufener,[72] proposed a model to study the Brownian motion of microspheres in a single relaxation time Maxwellian fluid, which was exemplified with a WM solution. They introduced a memory function in the Langevin equation of the form $\zeta(t) = (\zeta/\tau)e^{-t/\tau_M}$; $\zeta = 6\pi\eta_m R$, and η_m is the zero shear viscosity. In addition by

using DWS, they showed that the MSD of polystyrene microspheres embedded in a WM water solution, made of (0.27 M) cetyltrimethylammonium bromide (CTAB) and (0.5–2.5 M) KBr, are well described by that model at long times (low frequencies), at various temperatures. Particle motion was examined at short and long times, as well as at the plateau region, revealing the existence of an elastic response; the plateau was used to estimate G_0. The Maxwell fluid parameters (G_0 and τ_M) were of the same order of magnitude as those obtained by mechanical rheology. The Brownian motion in a Maxwell fluid has been recently revisited[73] to study the role of hydrodynamic memory and its interplay with medium viscoelasticity, where the velocity autocorrelation function was identified as a sensible quantity encoding that interplay. In concentrated WM aqueous solutions, made of hexaethyleneglycol mono n-hexadecyl ether ($C_{16}E_6$),[74] the MSD, $G'(\omega)$, and $G''(\omega)$ were determined from $T = 28$ °C to $T = 36$ °C, using a combination of single- and multispeckle DWS with polystyrene microspheres as tracers. The accessible range of microrheology was extended by several orders of magnitude. In this case, a correction factor of 1.52–2 of unknown origin was necessary to obtain a quantitative agreement between optical microrheology and classical mechanical rheometry. The MSD was measured for polystyrene particles embedded in WM solutions made of hexane sulfonate cetyltrimethyl ammonium ($CTAC_6SO_3$), and of heptane sulfonate cetyltrimethyl ammonium ($CTAC_7SO_3$) both in water, in the semidilute regime, using DWS.[75] Three different regimes for the particle motion were described: (a) At short times, the particles diffuse freely in the solvent with a Brownian dynamics. (b) At intermediate times, the MSD remains constant for a given time interval, where particles are in Brownian motion trapped in a cage, and (c) at longer times, the motion again becomes diffusive. Here, the long-time diffusion coefficient corresponded to the macroscopic viscosity of the WM solution. They introduced a function that describes the MSD of particles in WM solutions over 10 decades in time (See Fig. 4a):

$$\left\langle \Delta r^2(t) \right\rangle = 6\delta^2 \left(1 - e^{-\left(\frac{D_0}{\delta^2} t\right)^{\alpha}} \right)^{1/\alpha} \left(1 + \frac{D_m}{\delta^2} t \right). \quad (5)$$

Here, $6\delta^2$ is the value of $\langle \Delta r^2(t) \rangle$ at the plateau where δ^2 corresponds to the cage size, D_o is the diffusion coefficient for particles in the solvent at infinite dilution, and D_m is the diffusion coefficient for the particles at long times. α accounts for the broad spectrum relaxation times at the plateau onset time. This procedure allowed to relate the cage size to the elastic modulus ($\delta^2 = k_B T/[6\pi R G_o]$). From the measured MSD, $G'(\omega)$ and $G''(\omega)$ were evaluated (using eqn (3)); they are in excellent agreement with mechanical rheology. A detailed comparison among the results of 1PMR, tracking optically trapped silica particles using back-focal plane interferometry, and macroscopic mechanical rheological technique, which used a piezorheometer over a frequency range from ~0.1 Hz to ~10 KHz, was carried out in the WM solution made of cetyl pyridinium choride (CpyCl) and the strongly binding counterion sodium salicylate (NaSal) in brine (0.5 M), at a molar ratio NaSal/CpyCl = 0.5.[20] An excellent agreement was found between microrheology and mechanical rheology. In a next paper,[17] the same group presented a quantitative comparison among 1PMR, 2PMR, and mechanical microrheology using a high frequency piezorheometer in a range $\sim 10^{-1}$ and 5×10^4 Hz. The agreement between all techniques was excellent, although the 2PMR data were noisier. The major disagreement between macro- and microrheology data is at frequencies < 1 Hz. The authors concluded that the agreement between micro- and macrorheology would be good if three conditions are met in the WM system: (1) The WM solution must be homogeneous on the scale of the particle size. (2) The particle should not perturb the local environment in which it moves on a scale comparable to its own size, *i.e.*, the particle size has to be much larger than any network length scale such as ξ or l_p. (3) There should be a non-slip boundary condition between the micelles and the particle surface. The good agreement between 1PMR and 2PMR demonstrates that local perturbation around the probes such as depletion, enrichment, or slip boundary conditions did not occur to a measurable degree, because 2PMR does not depend on the size or shape of the tracer particle and it is independent of the coupling between the tracer and the medium.

The next step forward to obtain characteristic lengths in WM networks is due to Willenbacher *et al.*[61] They showed that high frequency rheology can be used to determine structural and dynamic properties in WM solutions. At high frequencies, stress relaxation first is dominated by the Rouse-Zimm modes and then by the internal relaxation of individual Kuhn segments. This change occurs at the critical frequency ω_0 mentioned above. They studied the very well known system made of WM of CpyCl (100 mM) and Na Sal (60 mM), in water at different temperatures, using DWS and macroscopic mechanical rheometry (rotational rheometry, oscillatory squeeze flow, and torsional resonance oscillation). The agreement between DWS and mechanical rheometry is good, although the absolute values of $G'(\omega)$ and $G''(\omega)$ coming from DWS are 10%–20% lower than those from mechanical measurements. From their data, they obtained $l_p =$ 31–34 nm depending on the temperature, as well as $\xi \sim 52$ nm, and E_c.

Because of the validation success of microrheological techniques, and their capability to give experimental information to evaluate WM network characteristic lengths, a next stage started. Now, the interest of researchers is moving to get a better understanding of the behavior of WM solutions, particularly when the surfactant structure, counterion type, added electrolytes, relative concentration, or temperature are varied. The very well known WM water solution made of CTAB and NaSal has been studied with DWS, at different temperatures and NaSal/CTAB ratios.[30] From the time evolution of the MSD of embedded particles, $G'(\omega)$ and $G''(\omega)$ were obtained at high frequencies. This allowed to estimate all the characteristic lengths of the WM network and how they vary with the NaSal/CTAB ratio and T. Depending on the thermodynamic conditions, l_p ranged between ~ 29 and 36 nm, $l_e \sim$ 39–75 nm, and $L_c \sim$ 400–4800 nm. In this system, the larger the temperature, the smaller L_c. Afterwards, the WM solution of CpyCl (100 mM) and NaSal was revisited to study the linear-to-branched micelle transition.[76] The study was done at different NaSal/CpyCl ratios (0.5–5) and at frequencies from 10^{-2} to 10^6 rad/s using DWS and oscillatory squeeze flow generated with a piezo driven vibrator. It was found a quantitative agreement between mechanical high frequency

rheometry and DWS; however, G_o from DWS deviates from mechanical rheology as NaSal increases, as in other systems.[30] In this study, E_{sc}, ξ, and l_p ($\sim$ 26–30 nm) were calculated. This WM solution exhibits two maxima in the zero-shear viscosity and in τ_M when the salt/surfactant ratio is varied. It was concluded that the first maximum could be attributed to a transition from linear to branched micelles, the second viscosity increase to a decrease of the branching density accompanied by an increase of L_c, and the second viscosity decrease to a shortening of the WMs with an increase in the branching density. The variation of l_e, l_p, L_c, ξ and E_{sc} in WMs formed in water solutions of CTAB in the presence of different nonpenetrating counterions (Br^-, $NO3^-$, and $ClO3^-$) has been also investigated,[77] using mechanical high-frequency rheology and DWS at different salt/surfactant ratios. The results were compared with WMs made of CpyCl and the penetrating counterion NaSal. In general, the agreement between mechanical and optical methods is good. E_{sc},$\sim$ 17–20 k_BT, is independent of ionic strength and of the binding strength of the salt for systems with nonpenetrating counterions, and it is slightly higher compared to the system CpyCl/NaSal. l_p strongly depends on the nature of the salt, their values are $\sim$ 40, 34, and 29 nm for the systems CTAB/KBr, CTAB/$NaNO_3$, and CTAB/$NaClO_3$, respectively. Persistence lengths are also independent of the salt/surfactant ratio and also significantly higher than in the case of CpyCl/NaSal. Recently, the WM fluid made of a zwitterionic surfactant N-tetradecyl-N,N-dimethyl-3-ammonio-1-propanesulfonate (TDPS), sodium dodecyl sulfate (SDS), and salty water has been studied to get structural and dynamical information of the micellar network using DWS.[78] In this study, the MSD of embedded particles were obtained and $G'(\omega)$ and $G''(\omega)$ were evaluated. A detailed comparison of measurements for G_o and for τ_M obtained with DWS and with mechanical rheometry was done. On the average, the difference between DWS measurements with respect to mechanical rheometry is of $\sim$ 20% for G_o, and $\sim$ 35% for τ_M. In a general way, the values for G_o and τ_M are always lower when measured with DWS than when measured with mechanical rheometry. The agreement between both kinds of measurements was good, although it was not excellent. One point discussed by the authors was related to noticing that protocols for sample preparation play a central role. Cell geometry, cell parameters, sample preparation, and even different reactive stocks have been described as factors that could introduce deviations in WM mechanical rheology. In mechanical rheology, it is not strange that measurements for different nominally identical samples have an error bar of $\sim$ 20% for G_0 and of $\sim$ 5% for τ. In DWS microrheology, it is usual for a WM sample that is measured in different days to have an error bar of $\sim$7% for G_0 and of $\sim$ 8% for τ_M. Therefore, DWS microrheology seems to share some of these problems (sample preparation, probe particle dispersion method, *etc.*), and this has to be considered when DWS microrheology and mechanical rheology are compared. There are several factors that have been mentioned in the literature that could explain the difference, but neither of them is completely satisfactory. It has been suggested that hydrotope salt ions in solutions could be the responsible of this deviation,[30] but this suggestion was not supported by latter experimental work.[76] Local structure formation or surfactant adsorption hindering the tracer motion could be a possible scenario, which could modify the parameters obtained with DWS, but this needs further research. In this study, the WM network structural parameters were estimated from $G'(\omega)$ and $G''(\omega)$, *i.e.*, $6\delta^2$, l_e, l_p, L_c, ξ, for different surfactant ratios ([*SDS*]/[*TDPS*]), salt concentrations, and temperatures. ξ, l_e, l_p, were almost insensible to the change of these variables. In contrast, L_c was shorter as temperature increased: entropic contribution induces smaller micelles. When the surfactant ratio changes, L_c presents a peak at a ratio of $\sim$ 0.50–0.55. When the ionic strength of the media is increased though salt addition, L_c presents a peak at a salt concentration of $\sim$ 0.225 M. In some solutions, this length can reach values of $\sim$ 12 μm. Scission energies helped to understand why the contour length first increases and then decreases, when salt is added.

Now, microrheology is giving a different perspective to the study of WM solutions. It can allow making systematic studies to get a better understanding on how the physicochemical conditions transform micellar networks, and how these networks modify the rheological behavior. As examples, we have mentioned the study of the effect of penetrating or not penetrating counterions into the WM structure,[77] or the study of the effect of salt addition on the characteristic lengths of the WM network.[78] However, the study of the transition from linear to branched micelles[76] presents different challenges related to WM theory, and the way the results are interpreted. These issues have been difficult to explore until now. In nonionic surfactants in water, as the temperature increases, more branched networks are formed; whereas linear micelles appear at lower temperatures.[50] This anomalous behavior apparently is due to the effect of temperature on the spontaneous curvature, rather than to the energy/translational entropy balance. In ionic surfactants, when salt is added, the electrostatic repulsions between head groups are screened, inducing a linear growth; atomistic molecular dynamics simulations have clearly shown this effect.[79] However, after a maximum, salt addition suggests a decrease in the micellar size. Nevertheless, there are salty solutions with long WMs that exhibit an amazingly high fluidity that can not be accounted for the reptation model.[57] Two mechanisms have been proposed, although they have not critically examined yet.[80,81] In these mechanisms, local stress relaxes instead of disentangling through a mixture of reptation or breakage and recombination,[57] it relaxes by sliding the cross-links along the micelles through the viscous flow on the surfactant molecules, or by other processes that occur when micellar threads collide. In the latter, WMs form transient cross-links recombining on the other side of the encountered micelles after collision, to reform the WMs (ghost-like crossing).

Notwithstanding the success of microrheology, there are important questions related to how accurate the characteristic lengths of the WM networks coming from results of microrheology are. We need further research to make comparisons among characteristic lengths coming from microrheology and from other techniques, as SANS or by direct observation of individual WMs. Imaging of individual WMs made of diblock copolymers, doped with a hydrophobic fluorescent dye with fluorescence microscopy, has been possible in a microfluidic cross-flow device that creates an elongational flow;[82] L_c can be obtained and with further analysis, probably l_p could also be obtained.

4. Studies of Microrheology in suspensions embedded with F-actin and bacteriofhage fd

4.1. F-actin

Cells sense, generate, and respond to forces in their environment through cytoskeletal dynamics. An understanding of cytoskeletal mechanical properties would be essential for understanding cell mechanics and the associated biological phenomena. Cell experiments have revealed that the cytoskeleton exhibits both elastic and viscous characteristics under applied stress.[83,84] One of the principal constituents of the cytoskeleton is filamentous actin (F-actin). Structural assembly of F-actin is regulated by over 100 actin-binding proteins,[85] which organizes it in cross-linked networks and in bundled filaments. The later contributes to the structural stability of the cell, providing added mechanical strength. F-actin has raised much interest because understanding its mechanical behavior is of central importance for establishing how it works as a dynamic mechanical scaffold within living cells, to control many functions.

F-actin is a two-stranded helix ($d \sim 7$–8 nm) made of polymerized protein subunits, the actin monomers (G-actin). These filaments can become very long, $L_c \sim 10$–20 μm, and they are semiflexibe polymers on the micrometer scale, $l_p \sim 17$ μm.[86] Solutions of these filaments also are characterized by the average distance between filaments or the mesh size, ξ. The shear moduli of F-actin solutions have been determined by passive microrheology, through evaluating the power spectral density of position fluctuations of embedded particles, at various concentrations,[18] and with DWS;[87,98] F-actin L_c was not controlled in these studies. The agreement between mechanical and DWS measurements is good, at least over the frequency range probed by both instruments (within 10–15%). The elastic modulus dominates viscoelasticity at small frequencies, and the loss modulus dominates at large frequencies. The high-bandwidth measurements of the MSD were sensitive to both the fast bending fluctuations of single actin filaments at short times, and the macroscopic viscoelasticity of F-actin networks at long times, where the microsphere probes become elastically trapped by the actin filaments. At high frequencies, viscoelastic moduli scale as $\sim \omega^{\alpha}$, where $\alpha \sim {}^3\!/_4$. This exponent is much larger than that predicted for flexible polymer solutions $\alpha = {}^1\!/_2$. This unusual exponent, ${}^3\!/_4$, corresponds rather to a model of high-frequency dynamics of semi-flexible polymer solutions,[88] and it is a direct consequence of the finite rigidity of F-actin. With the development of 2PMR, it has been suggested that earlier interpretations using particle tracking, carried out with 1PMR, may not reflect the true bulk behavior.[14,15] 1PMR and 2PMR were used to probe the length scale dependence of the F-actin network microrheology, between 0.01–30 rad/s.[89] The contribution of the longitudinal fluctuations of the filaments, which lead to an increase the in elastic modulus at length scales up to l_p, was determined with 2PMR. With 1PMR, it was probed that the filament entanglement leads to a frequency-independent elastic modulus. Comparisons among results coming from active 2PMR and 1PMR, and passive microrheological methods for F-actin and actin driven by myosin motor proteins have been carried out.[23] In equilibrium, active and passive methods give the same results in the frequency range where both methods are reliable. In non-equilibrium systems, the combination of both methods provides an accurate method to quantify non-thermal fluctuations, and to calculate the spectrum of the forces driving the system out of equilibrium. One of the most interesting contributions to exploit microrheology in thread-like systems, allowing a better understanding of the mechanical response of entangled F-actin solutions at length scales from 1–100 μm, was in a study where both ξ and L_c where varied in a controlled way.[90] It was found that 1PMR probed the viscoelastic behavior at length scales of $\sim 2R$. For $\omega > \tau_c^{-1}$ (τ_c is the relaxation time of bending fluctuations over an entanglement length), $G'(\omega)$ and $G''(\omega)$ are remarkably insensitive to L_c, showing a frequency dependence that is compatible with $\omega^{3/4}$. This suggests that 1PMR probes bending fluctuations of single filaments at these frequencies. In this regime, single-filament dynamics dominate the mechanical response until filaments become sterically hindered at a length l_e. At frequencies $\omega < \tau_c^{-1}$, 1PMR shows an elastic plateau for samples with the longest filaments. This elastic plateau results from a steric hindrance of the filaments at a length l_e. In contrast, 2PMR shows an enhanced viscoelastic relaxation, which is filament-length dependent at intermediate frequencies. The relaxation time of this extra dissipation can be related to fluctuations in the quantity of material present in each segment of l_e; these density fluctuations diffuse along the filament. 2PMR shows that this additional relaxation leads to $G'(\omega) \sim G''(\omega) \sim \omega^{1/2}$. This scaling behavior has not been predicted theoretically. This study concluded that in entangled F-actin solutions, the mechanical response changes as the length scales in the system vary. Therefore, microrheology can be used to probe length-scale-dependent rheology. Moreover, the results also suggest that 1PMR may be more useful for measurements of cross-linked networks of semiflexible filaments, where contributions from long wavelength longitudinal fluctuations are reduced. The results highlight the sensitivity of the rheology of entangled solutions of semiflexible polymers to the length scales that determine both network geometry and filament properties; this provides new insight into the origin of the scaling behavior of rheology that has to be fully described theoretically. Quite recently, the effect of ABPs on the mechanical properties of homogeneous F-actin networks using both passive and active microrheology has been studied to correlate mechanical properties with structural geometry.[24] The microscale non-linear behavior of the cross-linked F-actin network was obtained by active measurement at high strain. The effects of length scale on both network elasticity and microstructure were investigated by controlling actin filament length and probe size, and it was showed that short actin filaments influence connectivity of the network structure resulting in a reduced elasticity.

4.2. Bacteriophage fd

Water suspensions of filamentous bacterial viruses with semiflexible structures where $L_c \sim L_p \gg d$ (See Fig. 5), is another system of recent interest. In particular, bacteriophage fd suspensions are quite attractive because they form liquid crystals at specific ranges of concentration and ionic strength;[91,92] a review can be found in ref. 93. In addition, they present a complicated nonlinear rheology,[94,95] exhibiting shear- and

vorticity-banding, and tumbling regimes, as well as interesting features when mixed with temperature-sensitive polymers as poly-N-isopropylacrylamide.[96] fd virus is an excellent model of an entangled network of monodisperse semiflexible filaments, which consists of a single-stranded circular DNA covered with a coat made of identical protein subunits, with $L_c \sim 0.9$ μm, $d \sim 7$ nm, and $l_p \sim 2.2$ μm. The viscolastic properties of suspensions of bacteriophage fd have been measured using both mechanical rheometry and active microrheology, which have been performed using a magnetic tweezers rheometer and particle tracking.[97] The study was mainly addressed to get $G'(\omega)$ and $G''(\omega)$ in the low frequency range ($\sim 0.06 < \omega < 25$ rad/s) for solutions in a concentration range of 5–15 mg/mL; $G''(\omega) > G'(\omega)$ for all frequencies below 6.2 rad/s. At frequencies above 6.2 rad/s, a shallow and slanted plateau-like region was found (~ 0.32 rad/s) for $G'(\omega)$ where $G'(\omega) \sim G''(\omega)$. $G''(\omega)$ exhibits an inflection point around 6.2 rad/s. In the low frequency regime, it was found that $G' \sim \omega^{0.9-1.2}$ and $G'' \sim \omega^{0.7-0.9}$, which are far from the expected behavior $G' \sim \omega^2$ and $G'' \sim \omega^1$. fd virus solutions have also been studied in the dilute, semidilute, and concentrated regimes ($c_{fd} \sim 0.2$–14 mg/mL) at an ionic strength $I = 50$ mM.[21] Here, $G'(\omega)$ and $G''(\omega)$ were measured in a wide frequency range ($0.62 < \omega < 6.2 \times 10^4$ rad/sec) using a passive microrheology method, evaluating the power spectral density of the thermal fluctuations of embedded particles, focused with a laser beam. In the dilute regime, $G^*(\omega)$ is dominated by the rigid rod rotational relaxation. Increasing the fd concentration, both moduli increase. Just below the isotropic-nematic phase transition, the elastic modulus is ~10 Pa, and the sample is still mainly viscous, *i.e.*, it remains rather weakly entangled. This was attributed to the relative short virus contour length and to the charged surface of the fd virus, which prevents sticking between them. Varying the fd concentration showed that entanglement becomes relevant only at concentrations beyond 2 mg/ml. In the high-concentration regime, at high frequencies, suspensions reflect a single semiflexible filament dynamics; at the high-frequency end, $G''(\omega) \sim \omega^{3/4}$ as predicted for semiflexible polymers. Notwithstanding that the viscoelastic properties of fd suspensions have been measured at low and at relatively high frequencies, there are many studies to be done. Suspensions of fd virus at higher concentrations or at higher ionic strength have not been explored. It would be appropriate that 1PMR and 2PMR experiments could be carried out, because it is not known the length scale dependence of the microrheology in these suspensions, as in the case of in F-actin solutions.

5. Concluding remarks

In this brief review, we have shown the way microrheology has evolved and it is becoming a reliable method to characterize the linear viscoelastic properties in soft matter. We have drawn attention to the new kind of investigations microrheology is allowing to develop in solutions with embedded thread-like supramolecular structures. Rheology in soft matter is now available in a very wide frequency interval, mechanical response at different length scales can be explored, rheological studies can be done in heterogeneous systems and particularly in biological matter. In particular, microrheology can be of help to enhance our understanding in wormlike micellar solutions, providing a relatively simple experimental method to obtain the characteristic lengths of the wormlike micellar network.

Acknowledgements

Funds from SEP-CONACYT (81081) and DGAPA-UNAM (112508) are gratefully acknowledged.

References

1 G. Maret, *Curr. Opin. Colloid Interface Sci.*, 1997, **2**, 251.
2 T. Gisler and D. A. Weitz, *Curr. Opin. Colloid Interface Sci.*, 1998, **3**, 586.
3 F. C. MacKintosh and C. F. Schmidt, *Curr. Opin. Colloid Interface Sci.*, 1999, **4**, 300.
4 A. Mukhhopadhyay and S. Granick, *Curr. Opin. Colloid Interface Sci.*, 2001, **6**, 423.
5 J. L. Harden and V. Viasnoff, *Curr. Opin. Colloid Interface Sci.*, 2001, **6**, 438.
6 F. Scheffold, S. Romer, F. Cardinaux, H. Bissig, A. Stradner, L. F. Rojas-Ochoa, V. Trappe, C. Urban, S. E. Skipetrov, L. Cipelletti and P. Schurtenbeger, *Prog. Colloid Polym. Sci.*, 2004, **123**, 141.
7 T. A. Waigh, *Rep. Prog. Phys.*, 2005, **68**, 685.
8 P. Cicuta and A. M. Donald, *Soft Matter*, 2007, **3**, 1449.
9 N. Willenbacher and C. Oelschlaeger, *Curr. Opin. Colloid Interface Sci.*, 2007, **12**, 43.
10 T. D. Squires and T. G. Mason, *Annu. Rev. Fluid Mech.*, 2010, **42**, 413.
11 M. L. Gardel, M. T. Valentine, D. A. Weitz. Microrheology. In: *Microscale Diagnostic Techniques*, K. S. Breuer (Ed). (Springer, Berlin, 2005). (Chap 1). p 1.
12 T. G. Mason and D. A Weitz, *Phys. Rev. Lett.*, 1995, **74**, 1250.
13 T. G. Mason, *Rheol. Acta*, 2000, **39**, 371.
14 J. C. Crocker, M. T. Valentine, E. R. Weeks, T. Gisler, P. D. Kaplan, A. G. Yodh and D. A. Weitz, *Phys. Rev. Lett.*, 2000, **85**, 888.
15 I. Y. Wong, M. L. Gardel, D. R. Reichman, E. R. Weeks, M. T. Valentine, A. R. Bausch and D. A. Weitz, *Phys. Rev. Lett.*, 2004, **92**, 178101.
16 L. D. Landau, E. M. Lifshitz. *Statistical Physics*. 3rd Ed. (Buttterworth and Heinemann. Oxford, 1980).
17 M. Buchanan, M. Atakhorrami, J. F. Palierne and C. F. Schmidt, *Macromolecules*, 2005, **38**, 8840.
18 F. Gittes, B. Schnurr, P. D. Olmsted, F. C. MacKintosh and C. F. Schmidt, *Phys. Rev. Lett.*, 1997, **79**, 3286.
19 B. Schnurr, F. Gittes, F. C. MacKintosh and C. F. Schmidt, *Macromolecules*, 1997, **30**, 7781.
20 M. Buchanan, M. Atakhorrami, J. F. Palierne, F. C. MacKintoch and C. F. Schmidt, *Phys. Rev. E: Stat., Nonlinear, Soft Matter Phys.*, 2005, **72**, 11504.
21 K. M. Addas, C. F. Schmidt and J. X. Tang, *Phys. Rev. E: Stat., Nonlinear, Soft Matter Phys.*, 2004, **70**, 21503.
22 R. R. Brau, J. M. Ferrer, H. Lee, C. E. Castro, B. K. Tam, P. B. Tarsa, P. Matsudaira, M. C. Boyce, R. D. Kamm and M. J. Lang, *J. Opt. A: Pure Appl. Opt.*, 2007, **9**, S103.
23 D. Mizuno, D. A. Head, F. C. MacKintosh and C. F. Schmidt, *Macromolecules*, 2008, **41**, 7194.
24 H. Lee, J. M. Ferrer, F. Nakamura, M. J. Lang and R. D. Kamm, *Acta Biomater.*, 2010, **6**, 1207.
25 C. Gosse and V. Croquette, *Biophys. J.*, 2002, **82**, 3314.
26 K. C. Neuman and A. Nagy, *Nat. Methods*, 2008, **5**, 491.
27 D. A. Weitz, D. J. Pine, Diffusing-Wave Spectroscopy: in *Dynamic Light Scattering*. W. Brown (Ed.) (Oxford University Press, New York 1993), Chap. 16, p. 652.
28 D. J. Pine, D. A. Weitz, J. X. Zhu and E. Herbolzheimer, *J. Phys.*, 1990, **51**, 2101.
29 D. D. Kaplan, M. H. Kao, A. G. Yodh and D. J. Pine, *App. Optics*, 1993, **32**, 3828.
30 J. Galvan-Miyoshi, J. Delgado and R. Castillo, *Eur. Phys. J. E*, 2008, **26**, 369.
31 J. Galvan-Miyoshi and R. Castillo, *Rev. Mex. Fis.*, 2008, **54**, 257.
32 L. F. Rojas-Ochoa, D. Lacoste, R. Lenke, P. Schurtenberger and F. Scheffold, *J. Opt. Soc. Am. A*, 2004, **21**, 1799.

33 F. Scheffold, S. E. Skipetrov, S. Romer and P. Schurtenberger, *Phys. Rev. E: Stat. Phys., Plasmas, Fluids, Relat. Interdiscip. Top.*, 2001, **63**, 61404.
34 V. Viasnoff, F. Lequeux and D. J. Pine, *Rev. Sci. Instrum.*, 2002, **73**, 2336.
35 R. Carminati, R. Elaloufi and J. J. Greffet, *Phys. Rev. Lett.*, 2004, **92**, 213903.
36 I. A. Hasnain and A. M. Donald, *Phys. Rev. E: Stat., Nonlinear, Soft Matter Phys.*, 2006, **73**, 31901.
37 B. U. Felderhof, *J. Chem. Phys.*, 2009, **131**, 164904.
38 A. S. Khair and T. M. Squires, *Phys. Rev. Lett.*, 2010, **105**, 156001.
39 M. Tassieri, G. M. Gibson, R. M. Evans, A. M. Yao, R. Warren, M. J. Padgett and J. M. Cooper, *Phys. Rev. E: Stat., Nonlinear, Soft Matter Phys.*, 2010, **81**, 26308.
40 B. Sun, Y. Roichman and D. Grier, *Opt. Express*, 2008, **16**, 15765.
41 F. Ortega, H. Ritacco and R. G. Rubio, *Curr. Opin. Colloid Interface Sci.*, 2010, **15**, 237.
42 M. Wang and R. J. Hill, *J. Fluid Mech.*, 2009, **640**, 357.
43 M. Wang and R. J. Hill, *Soft Matter*, 2008, **4**, 1048.
44 J. A. van Heiningen, A. Mohammadi and R. J. Hill, *Lab Chip*, 2010, **10**, 1907.
45 I. Santamaria-Holek and J. M. Rubi, *J. Chem. Phys.*, 2006, **125**, 64907.
46 I. Santamaria-Holek, J. M. Rubi and A. Gadomsky, *J. Phys. Chem. B*, 2007, **111**, 2293.
47 L. M. Walker, *Curr. Opin. Colloid Interface Sci.*, 2001, **6**, 451.
48 S. Ezrabi, E. Tuval and A. Aserin, *Adv. Colloid Interface Sci.*, 2006, **128–130**, 77.
49 J. F. Berret. Rheology of Wormlike Micelles: Equilibrium Properties and Shear Banding Transitions, in: R. G., Weiss, P. Terech. (ed.). *Molecular Gels. Materials with Self-Assembled Fibrillar Networks*. (Springer, The Netherlands, 2006) p. 663.
50 N. Dan and S. A. Safran, *Adv. Colloid Interface Sci.*, 2006, **123–126**, 323.
51 C. A. Dreiss, *Soft Matter*, 2007, **3**, 956.
52 R. Zana, E. W. Kaler (ed.) *Giant Micelles: Properties and Applications*, (CRC Press, Florida, 2007).
53 S. M. Fielding, *Soft Matter*, 2007, **3**, 1262.
54 J. K. Dhont and G. W. Briels, *Rheol. Acta*, 2008, **47**, 257.
55 P. D. Olmsted, *Rheol. Acta*, 2008, **47**, 283.
56 S. Maneneville, *Rheol. Acta*, 2008, **47**, 301.
57 M. E. Cates, *Macromolecules*, 1987, **20**, 2289.
58 M. E Cates and S. J. Candau, *J. Phys.: Condens. Matter*, 1990, **2**, 6869.
59 M. E. Cates, *J. Phys. Chem.*, 1990, **94**, 371.
60 R. Granek and M. E. Cates, *J. Chem. Phys.*, 1992, **96**, 4758.
61 N. Willenbacher, C. Oelschlaeger, M. Schopferer, P. Fischer, F. Cardinaux and F. Scheffold, *Phys. Rev. Lett.*, 2007, **99**, 68302.
62 S. Lerouge, J. F. Berret. Shear-Induced Transitions and Instabilities in Surfactant Wormlike Micelles, in: K. Dusek, J. F. Joanny (Eds). *Polymer Characterization*. (Springer-Verlag, Heidelberg, 2010) p.1.
63 R. Gomez-Corrales, J. F. Berret, L. M. Walter and J. Oberdisse, *Langmuir*, 1999, **15**, 6755.
64 B. A. Schubert, E. W. Kaler and N. J. Wagner, *Langmuir*, 2003, **19**, 4079.
65 V. M. Garamus, J. S. Pedersen, H. Kawasaki and H. Maeda, *Langmuir*, 2000, **16**, 6431.
66 L. J. Magid, Z. Li and P. D. Butler, *Langmuir*, 2000, **16**, 10028.
67 C. Sommer, J. S. Pedersen, S. U. Egelhaaf, L. Cannavacciuolo, J. Kohlbrecher and P. Schurtenberger, *Langmuir*, 2002, **18**, 2495.
68 H. Seto, T. Kato, M. Monkenbusch, T. Takeda, Y. Kawabata, M. Nagao, D. Okuhara, M. Imai and S. Komura, *J. Phys. Chem. Solids*, 1999, **60**, 1371.
69 F. Nettesheim and N. J. Wagner, *Langmuir*, 2007, **23**, 5267.
70 T. Shikata, S. J. Dahman and D. S. Pearson, *Langmuir*, 1994, **10**, 3470.
71 H. von Berlepsch, L. Harnau and P. Reineker, *J. Phys. Chem. B*, 1998, **102**, 7518.
72 J. H. van Zanten and K. P. Rufener, *Phys. Rev. E: Stat. Phys., Plasmas, Fluids, Relat. Interdiscip. Top.*, 2000, **62**, 5389.
73 M. Grimm, S. Jeney and T. Franosch, *Soft Matter*, 2011, **7**, 2076.
74 F. Cardinaux, L. Cipelletti, F. Scheffold and P. Schurtenberger, *Europhys. Lett.*, 2002, **57**, 738.
75 M. Bellour, M. Skouri, J. P. Munch and P. Hébraud, *Eur. Phys. J. E*, 2002, **8**, 431.
76 C. Oelschlaeger, M. Schopferer, F. Scheffold and N. Willenbacher, *Langmuir*, 2009, **25**, 716.
77 C. Oelschlaeger, P. Suwita and N. Willenbacher, *Langmuir*, 2010, **26**, 7045.
78 E. Sarmiento-Gomez, D. Lopez-Diaz and R. Castillo, *J. Phys. Chem. B*, 2010, **114**, 12193.
79 Z. Wang and R. G. Larson, *J. Phys. Chem. B*, 2009, **113**, 13697.
80 J. Appel, G. Porte, A. Khatory, F. Kern and S. J. Candau, *J. Phys. II*, 1992, **2**, 1045.
81 S. J. Candau, A. Khatory, F. Lequeux and F. Kern, *J. Phys. IV, C1*, 1993, **3**, 197.
82 P. A. Stone, S. D. Hudson, P. Dalhaimer, D. F. Discher, E. J. Amis and K. B. Migler, *Macromolecules*, 2006, **39**, 7144.
83 A. R. Bausch, W. Moller and E. Sackmann, *Biophys. J.*, 1999, **76**, 573.
84 B. Fabry, G. N. Maksym, J. P. Butler, M. Glogauer, D. Navajas and J. J. Fredberg, *Phys. Rev. Lett.*, 2001, **87**, 148102.
85 C. G. dos Remedios, D. Chhabra, M. Kekic, I. V. Desova, M. Tsubakihara, D. A. Berry and N. J. Nosworthy, *Physiol. Rev.*, 2003, **83**, 433.
86 A. Ott, M. Magnasco, A. Simon and A. Libchaber, *Phys. Rev. E: Stat. Phys., Plasmas, Fluids, Relat. Interdiscip. Top.*, 1993, **48**, 1642.
87 A. Palmer, T. G. Mason, J. Xu, S. C. Kuo and D. Wirtz, *Biophys. J.*, 1999, **76**, 1063.
88 D. C. Morse, *Macromolecules*, 1998, **31**, 7030.
89 M. L. Gardel, M. T. Valentine, J. C. Crocker, A. R. Bausch and D. A. Weitz, *Phys. Rev. Lett.*, 2003, **91**, 158302.
90 J. Liu, M. L. Gardel, K. Kroy, E. Frey, B. D. Hoffman, J. C. Crocker, A. R. Bausch and D. A. Weitz, *Phys. Rev. Lett.*, 2006, **96**, 118104.
91 Z. Dogic and S. Fraden, *Phys. Rev. Lett.*, 1997, **78**, 2417.
92 Z. Dogic and S. Fraden, *Langmuir*, 2000, **16**, 7820.
93 Z. Dogic and S. Fraden, *Curr. Opin. Colloid Interface Sci.*, 2006, **11**, 47.
94 M. Lettinga and J. K. G. Dhont, *J. Phys.: Condens. Matter*, 2004, **16**, S3929.
95 K. Kang, M. Lettinga, Z. Dogic and J. K. G. Dhont, *Phys. Rev. E: Stat., Nonlinear, Soft Matter Phys.*, 2006, **74**, 26307.
96 F. Huang, R. Rotstein, S. Fraden, K. E. Kasza and N. T. Flynn, *Soft Matter*, 2009, **5**, 2766.
97 F. G. Schmidt, B. Hinner, E. Sackmann and J. X. Tang, *Phys. Rev. E: Stat. Phys., Plasmas, Fluids, Relat. Interdiscip. Top.*, 2000, **62**, 5509.
98 K. Rufener, A. Palmer, J. Xu and D. Wirtz, *J. Non-Newtonian Fluid Mech.*, 1999, **82**, 303.